Franziska Lübkemann, Timo C. Gusenburger, Dominik Hinrichs, Rasmus Himstedt, Dirk Dorfs and Nadja C. Bigall*

# Synthesis of InP/ZnS Nanocrystals and Phase Transfer by Hydrolysis of Ester

**Abstract:** The synthesis of highly luminescent non-toxic nanocrystals (NCs) and the subsequent phase transfer to aqueous solution by hydrolysis of the crystal-bound ester are presented. Therefore, the synthesis of the spherical semiconductor system InP/ZnS was modified by changing the sulfur precursor in the synthesis from 1-dodecanethiol to dodecyl 3-mercaptopropionate (D3MP). By employing D3MP both as sulfur precursor for the ZnS shell growth and as stabilizing ligand, the phase transfer from organic to aqueous solution can be performed easily. Instead of the usually employed ligand exchange with mercaptopropionic acid, the NCs are only shaken with a sodium borate buffer in order to obtain aqueous soluble NCs by hydrolysis of the ester. In future work, the NCs must be protected against aggregation and the long term stability has to be increased. The optical properties of the samples are investigated by UV/Vis and photoluminescence spectroscopy, and the morphology of the nanoparticles (NPs) before and after phase transfer is determined by transmission electron microscopy.

**Keywords:** hydrolysis of ester; ligands; nanocrystal; nanoparticles; phase transfer; saponification; water transfer.

## 1 Introduction

In past decades the interest in the synthesis of highly photoluminescent colloidal semiconductor nanoparticles with different shapes, sizes and compositions is severely increased [1–5]. Due to their versatile properties, there is a broad field of

**\*Corresponding author: Nadja C. Bigall,** Institute for Physical Chemistry and Electrochemistry, Leibniz Universität Hannover, Callinstraße 3A, 30167 Hannover, Germany; and Laboratory for Nano- and Quantum Engineering, Leibniz Universität Hannover, Schneiderberg 39, 30167 Hannover, Germany, e-mail: nadja.bigall@pci.uni-hannover.de
**Franziska Lübkemann, Timo C. Gusenburger, Dominik Hinrichs, Rasmus Himstedt and Dirk Dorfs:** Institute for Physical Chemistry and Electrochemistry, Leibniz Universität Hannover, Callinstraße 3A, 30167 Hannover, Germany; and Laboratory for Nano- and Quantum Engineering, Leibniz Universität Hannover, Schneiderberg 39, 30167 Hannover, Germany

applications e.g. in biochemistry, biological analysis, or electronic devices. In the field of biology and medicine water soluble fluorescent non-toxic nanoparticles are used as cell marker to enable the visibility of biological process in the human body [6–8]. Nowadays, there is a broad range of methodologies for nanoparticle synthesis. Generally, they can be divided in wet chemical preparation (in organic solvent e.g. hot-injection [9–11] or heating-up [12], in aqueous solvent e.g. by chemical precipitation [13–16]), solid-state preparation (e.g. ball milling [17, 18]), gas-phase preparation (e.g. furnace flow reactors [19, 20]) or deposition methods (e.g. or molecular beam epitaxy [21, 22]). The hot-injection method is mainly used for colloidal nanoparticle synthesis due to the high degree of control over shape and size [9, 10]. By controlling the shape and size of nanocrystals (NCs) it is possible to tune their optical properties [9, 10]. In addition, the wide range of accessible II–VI (e.g. CdSe [9, 23], CdTe [14], ZnSe and ZnS) and III–V semiconductors (e.g. GaP, GaAs and InP [24, 25]) gives rise to a broad range of optical properties. By combining two semiconductor systems in one NC, so-called nanoheterostructures can be synthesized. They can be, e.g. dot-in-rod shaped CdSe/CdS [1], CdSe/ZnS [26] or spherical core-shell NCs like CdSe/ZnS [4], InP/ZnS [5, 27, 28], Cu-Zn-In-S/ZnS [11]. This enables the possibility to protect the particle cores from e.g. oxidative processes and improves the optical properties like the photoluminescence quantum yield (PLQY). To make the semiconductor suitable for biological applications, however, the NCs must be soluble in aqueous solutions. Therefore, different techniques have been developed in recent years to receive water stable NCs, including ligand exchange reactions with thiol-based molecules [29–31] as well as encapsulation into hydrophilic or amphiphilic (e.g. silica [32, 33] and amphiphilic polymers [34–36]) materials. Recently, a new approach by using hydrolysis of crystal-bound esters on the nanocrystal surface for the phase transfer was introduced by the working group Macdonald [37, 38]. This approach associated the nanoparticle synthesis part, in which dodecyl 3-mercaptopropionate (D3MP) is used as sulfur precursor as well as crystal-bound ligand, with the subsequent phase transfer from organic to aqueous solution by hydrolysis of the crystal-bound ester. The previous works of the working group Macdonald show the synthesis of $Cu_2S$ and CdSe/ZnS NCs by using D3MP as sulfur precursor and crystal-bound ligand. Via a basic treatment the organic soluble NCs were transferred to aqueous solution by the hydrolysis of the ester. This method has the advantage, that the surface of the NCs are not affected by the hydrolysis of the ester in comparison to the usually used ligand exchange procedures for the phase transfer. For fluorescent NCs, this approach seems promising, since the interface between the semiconductor and the ligand has a high influence on the optoelectronic properties, and it is worth investigating the suitability of this method for highly luminescent non-toxic nanocrystal systems.

In the present work, we investigated the synthesis of organic soluble InP/ZnS NCs by the hot-injection method. Instead of the recently employed 1-dodecanethiol, here, we used D3MP both as the sulfur precursor and as capping ligand in the synthesis. We investigated the synthesis of highly luminescent organic soluble InP/ZnS NCs by using D3MP and the subsequent water transfer by saponification of the ester by using an alkaline solution. Due to the incorporation of the capping ligand in the ZnS shell of the InP/ZnS core shell particle surface, a significant decrease of luminescence through the creation of surface trap states by the phase transfer procedure could be excluded for large particles. Caused by insufficient stabilization due to crystal-bound mercaptopropionic acid of the phase transferred InP/ZnS NCs, they start to aggregate after some time in aqueous solution which has to be overcome in future work. The applied technique allows an easy transfer of the InP/ZnS NCs from organic to aqueous solution without a significant alteration of the optoelectronic properties like e.g. a decrease of the photoluminescent quantum yield (PLQY) in case of large particle sizes.

# 2  Experimental section

InP/ZnS NCs were synthesized by following the previous report from Reiss et al. with some modifications [5]. Instead of the reported one-pot one step synthesis, here the core/shell NCs were synthesized in a one-pot but two step synthesis. In the first reaction step InP core particles were synthesized by heating-up the reaction mixture under inert atmosphere. In the second step dodecyl 3-marcap-topropionate (D3MP) dissolved in octadecene was injected at 230 °C to grow a ZnS shell around the InP core. D3MP is sulfur precursor and stabilizing ligand at the same time. By using different amounts of myristic acid (MA) in the synthesis of the indium myristate precursor, different sizes of InP cores can be obtained. For the sake of clarity, we introduce the following abbreviations: InP/ZnS (S) for small InP core, InP/ZnS (M) for medium sized InP core and InP/ZnS (L) for large InP core. The amount of zinc and sulfur precursor was constant in all syntheses.

## 2.1 Chemicals

Indium(III) acetate (99.99%), zinc stearate (12.5–14%) purchased from Alfa Aesar. 1-dodecanol (98%), *n*-hexane (99%), 3-mercaptopropionic acid (99%), myristic acid (MA, 99%), 1-octadecene (ODE, 90%), potassium hydroxide (KOH, >85%), sulfuric acid (95–97%), tetrahydrofuran (THF, 99.9%) were purchased

from Sigma Aldrich. Tris(trimethylsilyl)phosphine (98%) was purchased from ABCR. Dichloromethane (>99.9%) 2-propanol (99.5%) purchased from Carl Roth. Magnesium sulfate ($MgSO_4$, 62–70%) was purchased from Fisher Chemical.

## 2.2 Synthesis of indium myristate In(MA)$_x$ stock solution

The indium myristate precursors were synthesized according to the procedure of Li and Reiss [5]. Two millimolar indium acetate, a varying quantity (2; 3; 4.3 mmol) of MA and 20 mL ODE were mixed in a three-neck flask equipped with condenser under inert atmosphere. The mixture was heated up to 120 °C for 2 h under vacuum, cooled down to room temperature, refilled with argon, and stored under inert atmosphere.

## 2.3 Synthesis of dodecyl 3-merctopropionate (D3MP)

D3MP was synthesized according to the procedure of Byrne et al. with some modifications [39]. Therefore, 3.5 mL 3-mercaptopropionic acid (20 mmol), 26.9 mL 1-dodecanol (60 mmol) and 10 drops of conc. $H_2SO_4$ were mixed in a screw cap vial and stirred over night at room temperature. The reaction mixture was diluted with dichloromethane and washed with distilled water. The organic phase was dried with $MgSO_4$ and evaporated. D3MP was obtained as colorless oil (24.03 g, 90.6%) and stored under inert atmosphere.

## 2.4 Synthesis of InP/ZnS core/shell NCs

One milliliter of In(MA)$_x$ (2 mmol, 3 mmol, 4.3 mmol) stock solution, 0.063 g zinc stearate, 7 mL ODE and 29 μL tris(trimethylsilyl)phosphine were mixed in a three-neck flask under inert atmosphere. For the InP core growth, the reaction mixture was kept under inert atmosphere for 30 min at 150 °C, subsequently for 1 h at 230 °C. 1 mL of the sample was taken with a glass syringe. Then, 40 μL of D3MP diluted in 500 μL ODE were injected, and the reaction mixture was heated 2 h at 230 °C followed by cooling to room temperature. All samples were precipitated with 10–15 mL 2-propanol, centrifuged (8000 RCF) and subsequently dissolved in 2 mL *n*-hexane. After that, 500 μL chloroform were added to the samples, followed by centrifugation to remove excess of organics. The samples were precipitated twice with 2-propanol, centrifuged and stored in *n*-hexane.

## 2.5 Preparation of water-soluble InP/ZnS NCs

One hundred microliters InP/ZnS NCs were precipitated with 1 mL 2-propanol, centrifuged 5 min (14.100 RCF), and redispersed in 2 mL THF. To decompose D3MP at the nanoparticle surface 100 µL of $Na_2B_4O_7 \cdot 10\,H_2O$ buffer solution (pH 9.3, 8.9 mL 0.1 M NaOH, 0.05 M sodium tetraborate decahydrate in 100 mL volumetric flask) were added. The reaction mixture was kept 2 h at 50 °C in an ultrasonic bath. The NCs were precipitated with 4 mL *n*-hexane and centrifuged for 5 min (6.000 RCF). Afterwards, the InP/ZnS NCs were washed with 4 mL ethanol and centrifuged again for 5 min (6.000 RCF). The cleaned NCs were dispersed and stored in water.

# 3 Characterization

## 3.1 Transmission electron microscopy

The morphology of the InP/ZnS NCs in solution was investigated by transmission electron microscopy (TEM) using a FEI Tecnai G2 F20 TMP ($C_S = 2$ mm, $C_C = 2$ mm) transmission electron microscope, equipped with a 200 kV field emission gun. Micrographs were taken in bright field mode. For the grid preparation, 10 µL of the purified and diluted sample were drop casted on a 300 mesh carbon coated copper grid, purchased from Quantifoil. The intensities of the selected area electron diffraction (SAED) ring patterns were azimuthal integrated utilizing the profile analysis of SAD (PASAD) plugin for Digital Micrograph [40, 41]. The raw profiles were exported without any background corrections.

## 3.2 Spectroscopic characterization

UV/Vis absorption spectra were recorded using a Cary 5000 absorption spectrophotometer equipped with an integrating sphere DRA-2500 from Agilent. The spectra were measured in hexane and dist. water and the concentration was adjusted to an optical density of 0.1 at the first absorption maximum from InP. Photoluminescence emission spectra were measured using a Horiba Fluoromax-4. PLQYs (measured in absolute mode by dividing the number of emitted photons by the number of absorbed photons) of the samples were recorded using a Dual-FL spectrophotometer equipped with a Quanta-ϕ integrating sphere pur-

chased from Horiba. All optical measurements were performed in fluorescence quartz cuvettes purchased von Hellma Analytics.

## 3.3 Powder X-ray diffraction

Powder X-ray diffraction (XRD) pattern were recorded using a Bruker D8 Advance in reflection mode with CuK$_\alpha$ source operating at 400 kV and 30 mA. For sample preparation 10 µL of the NP solution were drop casted several times on a crystalline silicon sample holder.

# 4  Results and discussion

In this work, we want to demonstrate the synthesis of InP/ZnS NCs by a modified synthesis route and the direct phase transfer after the synthesis due to hydrolysis of esters. The scheme in Figure 1 shows the synthetic route for the here presented InP/ZnS NP.

## 4.1 InP/ZnS nanoparticles

The transmission electron microscopic (TEM) images and size histograms from the as synthesized InP cores and InP/ZnS NCs are shown in Figure 2. The InP core NCs and the InP/ZnS NCs have a spherical shape and a narrow size distribution. For the InP core NCs the particle size varied from $2.1 \pm 0.5$ nm for small cores over $2.5 \pm 0.4$ nm for medium sized cores to $3.2 \pm 0.7$ nm for large InP cores. After ZnS
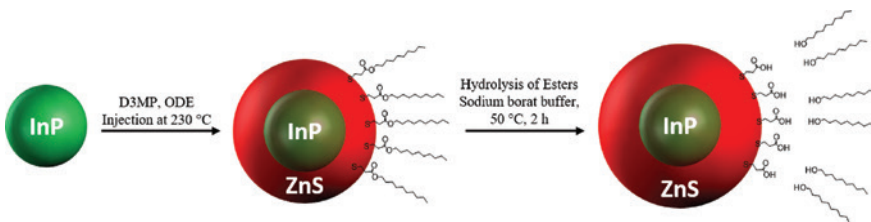


**Fig. 1:** Scheme of synthesis route. In first reaction step InP core NPs were formed. Due to the addition of D3MP as sulfur precursor and ligand, a ZnS shell was grown on the InP core. The last reaction step is the hydrolysis of the D3MP ester to phase transfer the particles from organic to aqueous solution.
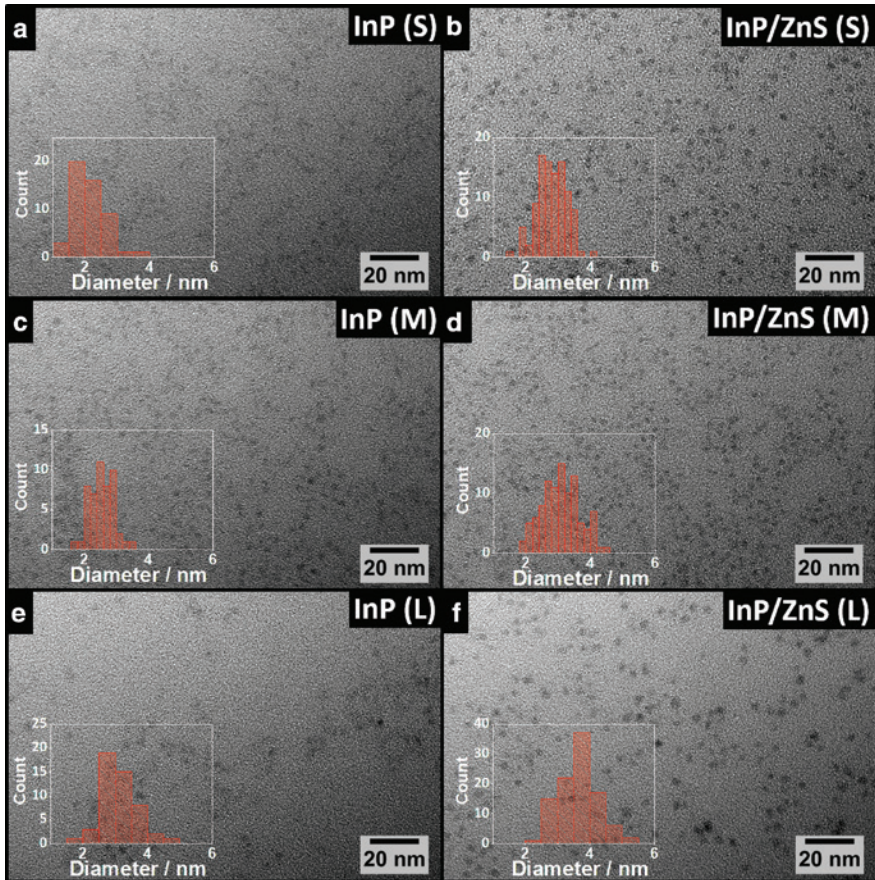
**Fig. 2:** TEM images with size histograms (inset) of InP core NCs and InP/ZnS NCs with different InP core sizes. (a) Small InP cores, (c) medium sized InP cores, (e) large InP cores, (b) InP/ZnS (S) with small InP cores, (d) InP/ZnS (M) NCs with medium sized InP core, (f) InP/ZnS (L) with large InP core.

shell growth the particle size increased and is within the range of $2.8 \pm 0.5$ nm for InP/ZnS (S) with a small InP core, $3.1 \pm 0.6$ nm for InP/ZnS (M) NCs with medium sized InP core and $3.6 \pm 0.6$ nm for InP/ZnS (L) NCs with a large InP core. Due to the low contrast, the difference between the InP core and the ZnS shell cannot be seen in the TEM images.

The crystal phase of the InP/ZnS NCs is identified by means of powder X-ray diffraction (XRD) measurements, which are shown in Figure 3. By comparing the measured XRD patterns (Figure 3a–c) to literature diffraction pattern (Figure 3d), the cubic phases from InP and ZnS can be assigned to the synthesized samples.
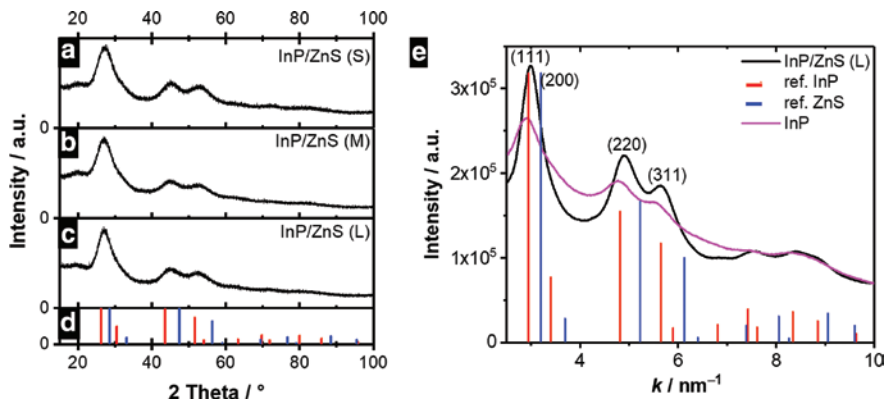
**Fig. 3:** Powder X-ray diffractograms of (a) InP/ZnS (S), (b) InP/ZnS (M), and (c) InP/ZnS (L) NCs. Diffraction pattern for comparison (d) of cubic InP (red) (PDF card No. 03-065-2889) and cubic ZnS (blue) (PDF card No. 03-065-1691). Electron diffraction (SAED) of InP and InP/ZnS (L) NCs (e).

Due to the similarity of the cubic InP and ZnS phase, electron diffraction (SAED) of the largest InP/ZnS NCs was measured to further proof the ZnS shell growth on the InP core. Therefore, electron diffraction was recorded from the InP core NPs and the InP/ZnS NPs. Both are shown in Figure 3e. It can be seen that the reflections (111), (200) and (311) of the InP/ZnS sample are shifted to shorter lattice distances in comparison to the pure InP sample, which was taken before the sulfur precursor was injected. This behavior is in line with a ZnS shell growth around the InP core NCs.

Additional, optical characterization (absorption and photoluminescence measurements) of the InP cores and the related InP/ZnS NCs were conducted and shown in Figure 4. In all obtained absorption spectra, a slight shift of the InP absorption band to higher wavelengths after the ZnS shell growth compared to the pure InP core absorption spectra can be seen. The InP absorption band shifted from 430 nm for small InP cores to 470 nm for InP/ZnS (S) NCs, from 480 nm for medium sized InP cores to 490 nm for InP/ZnS (M) NCs and from 530 nm for the large InP cores to 550 nm for InP/ZnS (L) NCs. This red shift with shell growth is an indicator that the charge carrier probability density function of the excited charge carriers spreads significantly into the shell materials despite of the high band gap of ZnS. Furthermore, in all cases a second absorption band and shorter wavelengths arises. This additional band is located at 420 nm for small InP/ZnS (S) NCs and medium sized InP/ZnS (M) NCs and at 430 nm for the large InP/ZnS (L) NCs. It appears after the shell growth and can be assigned to the ZnS. The emission band of the particles is located at at 526 nm for the InP/ZnS (S) NCs, at 542 nm for the InP/ZnS (M) NCs and at 616 nm for the InP/ZnS (L) NCs. This shift
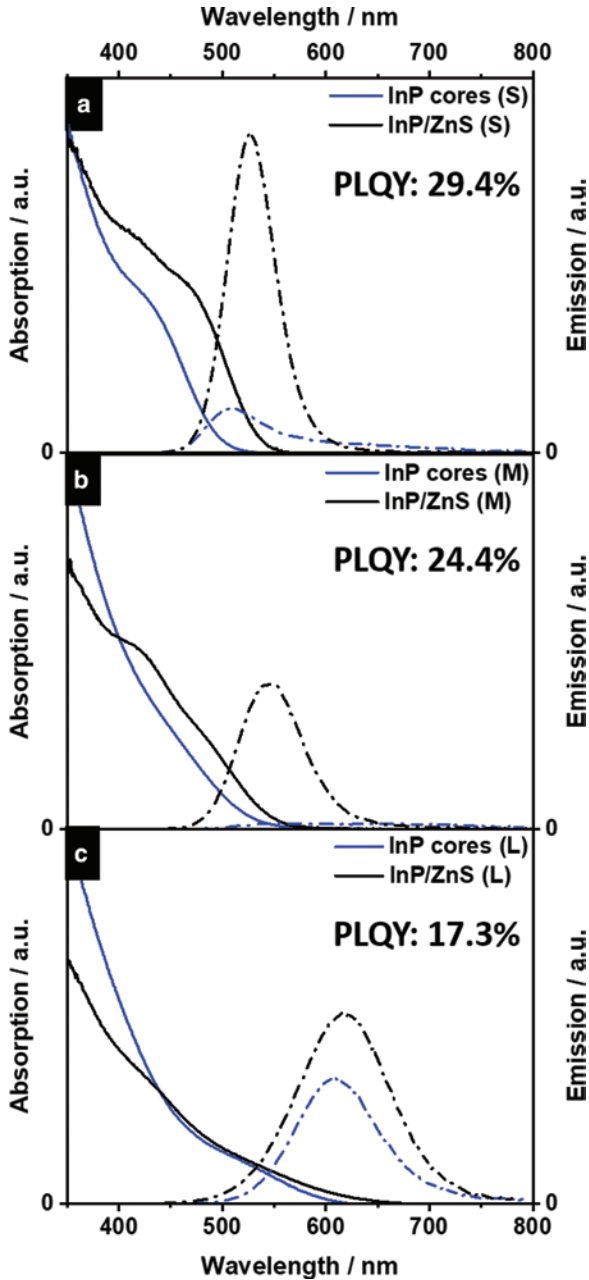
**Fig. 4:** Absorption spectra (solid lines) and emission spectra (dashed lines) of (a) small InP cores (blue) and InP/ZnS (S) NCs (black), (b) medium sized InP cores (blue) and InP/ZnS (M) NCs (black) and (c) large InP cores (blue) and InP/ZnS (L) NCs (black).

is simply explained by size quantization. The fwhm of the emission band of the larger particles is slightly broader than the fwhm of the smaller particles. Compared to the InP cores all emission maxima are shifted to higher wavelengths after ZnS shell growth. The photoluminescent quantum yield (29.4%, 24.4% and 17.3%) is decreasing with increasing particle size but always much higher for the core-shell particles than for the pure InP particles, since the ZnS effectively prevents charge carriers from being trapped at the particle surface.

## 4.2 Phase transferred InP/ZnS NCs

The optical characterization of the aqueous soluble InP/ZnS NCs (red lines) and the comparison to the organic solution (black lines) is shown in Figure 5. As can be seen, the slope of the absorption spectra and the absorption band position of the InP/ZnS core-shell particles is in all cases the same in organic and aqueous solution. This indicates, that the ZnS shell and the InP core are not strongly
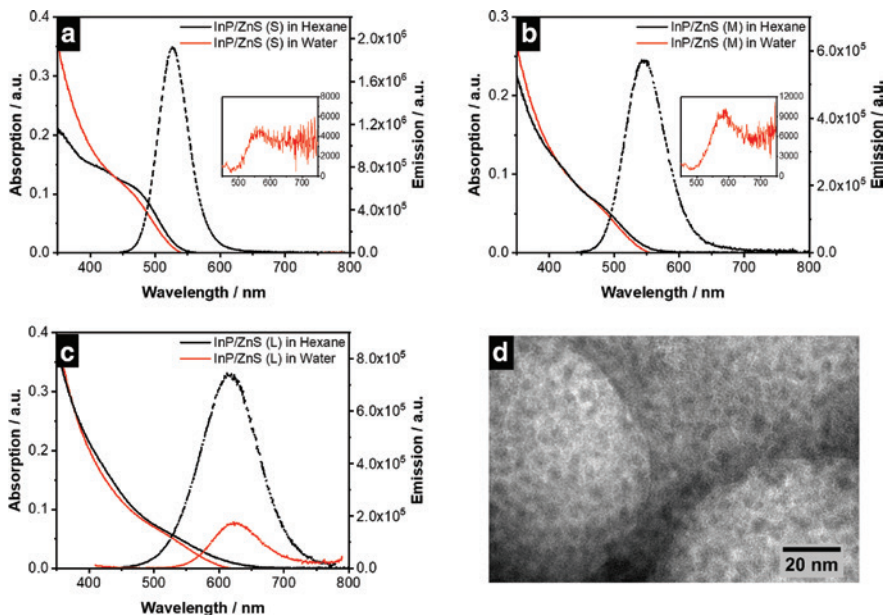


**Fig. 5:** Absorption- and emission spectra of organic solution (black line) and aqueous solution (red line) of (a) small InP/ZnS NCs (S), (b) medium sized InP/ZnS NCs (M) and (c) large InP/ZnS NCs (L). The insets in a and b show the magnification of the emission spectra of InP/ZnS NCs in aqueous solution. Transmission electron microscope image (d) of large aqueous soluble InP/ZnS NCs.

affected by the hydrolysis reagent. The emission maxima of the aqueous InP/ZnS NCs solutions shift in all cases to larger wavelengths and the emission intensities decreases. This shift becomes smaller with increasing particles size. One reason for the red shift can be changes in the coordination of Zn from stearate to hydroxide due to the base addition. The hydroxide anions are known to charge balance the surface of NCs. This new electron traps are localized surface defects and can change the electron wavefunction [42]. Furthermore, the addition of base can induce defects e.g. trap-states on the NC surface. This trap-states can also be a reason for a red-shift of the emission maxima. In all cases the emission intensity is decreasing from organic to aqueous solution. This decrease can also cause by trap-states on the NC surface. Another explanation for the decrease in emission intensity after the phase transfer can be the poor passivation against the environment due to the short length of the crystal-bound MPA. The PLQYs decrease after phase transfer from organic to aqueous solution. The quenching effect is higher with decreasing particle sizes. In case of the smallest InP/ZnS NCs it drops from 29.4% to 0.8%, at the medium sized NCs from 24.4% to 3.3% and at the larges InP/ZnS NCs from 17.2% to 10.6%. This observed tendency could be explained by the different magnitude of the probability density function of the charge carriers at the particle surface for the different InP core sizes. The smallest InP core will obviously show the strongest size quantization and hence the probability density function will leak strongly into the ZnS shell. Therefore, at the new surface of the core shell particle, the probability density function for the charge carriers will have a larger value for the smaller InP cores, resulting in a larger trapping probability. Hence, in future experiments, possibly thicker ZnS shells should be invoked when very small InP particles serve as core particles. The TEM image of the largest phase transferred InP/ZnS NCs are shown exemplarily in Figure 5d. Due to the strong aggregation on the TEM grid it was difficult to visualize the NCs. It can be seen, that the crystallinity due to the visible lattice planes and size of the large InP/ZnS (L) are not affected by the hydrolysis of the ester.

# 5 Conclusion

In this work we presented the synthesis of spherical InP/ZnS NCs with different sizes by using D3MP as sulfur precursor and ligand. The sizes are varied from 2.8 to 3.6 nm by the amount of the used indium myristate precursor and have a narrow size distribution. It was shown, that the variation in size also leads to variation of the optical properties. The obtained organic soluble InP/ZnS NCs show PLQY up to 29.4% for NCs with 2.8 nm diameter and 17.3% for NCs with

3.6 nm diameter. The InP/ZnS NCs were easily transferred to aqueous solution by hydrolysis of the surface bound D3MP esters by using a sodium borate buffer. The water soluble NCs show a decrease in the PLQY. Insufficient incorporation of crystal-bound D3MP in the ZnS shell could be avoided by reducing the reaction temperature and the reaction time of the shell growth. Even though future work has to be conducted in order to apply this strategy for obtaining optimum colloidal and optical properties, our work demonstrates a first step towards an easy synthetic route for phase transfer of highly luminescent non-toxic NCs direct after synthesis by hydrolysis of the crystal-bound ester.

# References

1.  L. Carbone, C. Nobile, M. De Giorgi, F. Della Sala, G. Morello, P. Pompa, M. Hytch, E. Snoeck, A. Fiore, I. R. Franchini, M. Nadasan, A. F. Silvestre, L. Chiodo, S. Kudera, R. Cingolani, R. Krahne, L. Manna, Nano Lett. **7** (2007) 2942.
2.  N. J. Borys, M. J. Walter, J. Huang, D. V. Talapin, J. M. Lupton, Science **330** (2010) 1371.
3.  S. Deka, K. Miszta, D. Dorfs, A. Genovese, G. Bertoni, L. Manna, Nano Lett. **10** (2010) 3770.
4.  B. O. Dabbousi, J. Rodriguez-Viejo, F. V. Mikulec, J. R. Heine, H. Mattoussi, R. Ober, K. F. Jensen, M. G. Bawendi, J. Phys. Chem. B **101** (1997) 9463.
5.  L. Li, P. Reiss, J. Am. Chem. Soc. **130** (2008) 11588.
6.  M. Bruchez Jr, M. Moronne, P. Gin, S. Weiss, A. P. Alivisatos, Science **281** (1998) 2013.
7.  K. E. Sapsford, T. Pons, I. L. Medintz, H. Mattoussi, Sensors **6** (2006) 925.
8.  O. T. Bruns, H. Ittrich, K. Peldschus, M. G. Kaul, U. I. Tromsdorf, J. Lauterwasser, M. S. Nikolic, B. Mollwitz, M. Merkel, N. C. Bigall, S. Sapra, R. Reimer, H. Hohenberg, H. Weller, A. Eychmüller, G. Adam, U. Beisiegel, J. Heeren, Nat. Nanotechnol. **4** (2009) 193.
9.  C. B. Murray, D. J. Norris, M. G. Bawendi, J. Am. Chem. Soc. **115** (1993) 8706.

10. M. Green, H. Harwood, C. Barrowman, P. Rahman, A. Eggeman, F. Festry, P. Dobson, T. Ng, J. Mater. Chem. **17** (2007) 1989.
11. J. F. L. Lox, F. Eichler, T. Erdem, M. Adam, N. Gaponik, H. V. Demir, V. Lesnyak, A. Eychmüller, Z. Phys. Chem. **233** (2019) 23.
12. J. van Embden, A. S. R. Chesman, J. J. Jasieniak, Chem. Mater. **27** (2015) 2246.
13. N. C. Bigall, T. Härtling, M. Klose, P. Simon, L. M. Eng, A. Eychmüller, Nano Lett. **8** (2008) 4588.
14. N. Gaponik, D. V. Talapin, A. L. Rogach, K. Hoppe, E. V. Shevchenko, A. Kornowski, A. Eychmüller, H. Weller, J. Phys. Chem. B **106** (2002) 7177.
15. M. Santhosh, T. Chitravel, R. Jayaprakasam, V. N. Vijayakumar, Z. Phys. Chem. **230** (2016) 1551.
16. A. Dumbrava, D. Berger, G. Prodan, F. Moscalu, A. Diacon, Z. Phys. Chem. **232** (2017) 61.
17. P. K. Giri, S. Bhattacharyya, D. K. Singh, R. Kesavamoorthy, B. K. Panigrahi, K. G. M. Nair, J. Appl. Phys. **102** (2007) 093515.
18. C. F. Burmeister, A. Kwade, Chem. Soc. Rev. **42** (2013) 7660.
19. H. G. Scheibel, J. Porstendörfer, J. Aerosol Sci. **14** (1983) 113.
20. I. W. Lenggoro, K. Okuyama, J. Fernández de la Mora, N. Tohge, J. Aerosol Sci. **31** (2000) 121.
21. Y. W. Heo, V. Varadarajan, M. Kaufman, K. Kim, D. P. Norton, F. Ren, P. H. Fleming, Appl. Phys. Lett. **81** (2002) 3046.
22. N. Uchitomi, H. Toyota, T. Takahashi, Z. Phys. Chem. **230** (2016) 499.
23. J. E. B. Katari, V. L. Colvin, A. P. Alivisatos, J. Phys. Chem. **98** (1994) 4109.
24. O. I. Mićić, J. Sprague, Z. Lu, A. J. Nozik, Appl. Phys. Lett. **68** (1996) 3150.
25. O. Zerzouf, M. Haase, Z. Phys. Chem. **221** (2007) 393.
26. T. Mokari, U. Banin, Chem. Mater. **15** (2003) 3955.
27. S. Xu, J. Ziegler, T. Nann, J. Mater. Chem. **18** (2008) 2653.
28. S. Haubold, M. Haase, A. Kornowski, H. Weller, ChemPhysChem **2** (2001) 331.
29. T. Kodanek, H. M. Banbela, S. Naskar, P. Adel, N. C. Bigall, D. Dorfs, Nanoscale **7** (2015) 19300.
30. S. F. Wuister, I. Swart, F. van Driel, S. G. Hickey, C. de Mello Donegá, Nano Lett. **3** (2003) 503.
31. W. R. Algar, U. J. Krull, ChemPhysChem **8** (2007) 561.
32. E. M. Hutter, F. Pietra, R. J. A. Van Dijk-Moes, D. Mitoraj, J. D. Meeldijk, C. De Mello Donegá, D. Vanmaekelbergh, Chem. Mater. **26** (2014) 1905.
33. X. Tang, E. Kröger, A. Nielsen, C. Strelow, A. Mews, T. Kipp, Langmuir **33** (2017) 5253.
34. T. Pellegrino, L. Manna, S. Kudera, T. Liedl, D. Koktysh, A. L. Rogach, S. Keller, J. Rädler, G. Natile, W. J. Parak, Nano Lett. **4** (2004) 703.
35. I. L. Medintz, H. T. Uyeda, E. R. Goldman, H. Mattoussi, Nat. Mater. **4** (2005) 435.
36. W. Wang, A. Kapur, X. Ji, M. Safi, G. Palui, V. Palomo, P. E. Dawson, H. Mattoussi, J. Am. Chem. Soc. **137** (2015) 5438.
37. M. J. Turo, J. E. Macdonald, ACS Nano **8** (2014) 10205.
38. M. J. Turo, X. Shen, N. K. Brandon, S. Castillo, A. M. Fall, S. T. Pantelides, J. E. Macdonald, Chem. Commun. **52** (2016) 12214.
39. C. Byrne, F. Sallas, D. K. Rai, J. Ogier, R. Darcy, Org. Biomol. Chem. **7** (2009) 3763.
40. C. Grammer, "http://www.univie.ac.at/pasad.," (2018).
41. C. Gammer, C. Mangler, C. Rentenberger, H. P. Karnthaler, Scr. Mater. **63** (2010) 312.
42. D. Zherebetskyy, M. Scheele, Y. Zhang, N. Bronstein, C. Thompson, D. Britt, M. Salmeron, P. Alivisatos, L.-W. Wang, Science **344** (2014) 1380.